PERGAMON

International Journal of Heat and Mass Transfer 46 (2003) 949–961

International Journal of HEAT and MASS TRANSFER

www.elsevier.com/locate/ijhmt

A reciprocal flow filtration combustor with embedded heat exchangers: numerical study

Fabiano Contarin, Alexei V. Saveliev, Alexander A. Fridman, Lawrence A. Kennedy *

Department of Mechanical Engineering, College of Engineering (M/C 159), University of Illinois at Chicago, 851 South Morgan Street, Chicago, IL 60607-7043, USA

Received 27 April 2002; received in revised form 7 September 2002

Abstract

A reciprocal flow filtration combustor with embedded heat exchangers is numerically studied. In this system the combustion of methane and air mixture is stabilized in a transient porous media combustor by periodical switching the direction of the flow. Two heat exchangers are placed in the terminal sections of the porous matrix, constraining the reaction in the central insulated zone. The predicted temperature profile inside the reactor has a typical trapezoidal shape. The central plateau temperature ranges between 1300 and 1600 K as the equivalence ratio varies from 0.15 to 0.7 and the filtration velocity from 15 to 45 cm/s. The efficiency spans the range of 50–80% being higher for higher equivalence ratios and filtration velocities.

1. Introduction

As an internally self-organized process of heat recuperation, filtration combustion of gaseous mixtures in porous media differs significantly from homogeneous flames. This difference can be attributed to two main factors: the highly developed inner surface of the porous media results in efficient heat transfer between the gas and the solid, and the intense mixing of the gas flow through the porous media increases effective diffusion and heat transfer in the gas phase.

Stationary and transient systems are the two major design approaches commonly employed in porous combustion. The first approach is widely used in radiant burners and surface combustor heaters. In such systems, the combustion zone is stabilized in a finite section of porous matrix by the imposed boundary conditions. However, in an unrestricted uniform porous media, the combustion zone can propagate freely as a combustion wave in either downstream or upstream directions.

Strong interstitial heat transfer results in low degree of thermal non-equilibrium between the gas and the solid phases that couples the thermal and the reaction wave. This situation generally corresponds to the low velocity regime of filtration gas combustion, according to classification given by Babkin [1]. The motion of the combustion zone results in positive or negative enthalpy fluxes between the reacting gas and solid carcass. As a result, observed combustion temperatures can significantly differ from adiabatic predictions based on the enthalpy of the initial reactants and are controlled mainly by the reaction chemistry and heat transfer mechanism. The upstream wave propagation, countercurrent to filtration velocity, results in underadiabatic combustion temperatures [2] while the downstream propagation of the wave leads to the combustion in superadiabatic regime with temperatures much in excess of the adiabatic [3]. Superadiabatic combustion significantly extends conventional flammability limits to the region of the ultra-low heat content mixtures. The combined effect of the lean mixtures and low combustion temperatures makes the superadiabatic burners

* Corresponding author. Tel.: +1-312-996-2400; fax: +1-312-996-8664.

E-mail address: lkennedy@uic.edu (L.A. Kennedy).

0017-9310/03/$ - see front matter
PII: S0017-9310(02)00371-X

Nomenclature

A	reactor cross-sectional area
A_f	Arrhenius pre-exponential factor
c	porous media specific heat
D	reactor diameter
d	packed bed pellet diameter
D_{ax}	axial dispersion coefficient
D_g	gas diffusion coefficient
E_a	activation energy
F	radiative heat exchange factor
H_{chem}	heat of chemical reaction
h_v	volumetric heat transfer coefficient
k	thermal conductivity
k_s^*	effective thermal conductivity of solid matrix
L	reactor length
LHV	low heating value
$\dot{m}$	mass flow rate of the gas mixture
Nu	Nusselt number
P	power per unit reactor area
Pr	Prandtl number
R	universal gas constant
Re	Reynolds number
T	temperature
v	velocity
x	axial coordinate
y_p	product mass fraction
W	volumetric products production rate

Greek symbols

β	heat loss coefficient
γ	mass fraction of CH_4 in the unburned stream
ε	porosity
ρ	density
σ	Stephan–Boltzmann constant

Subscripts

s	solid
g	gas
ex	extracted
i	interstitial
f	filtration
r	radiative
0	room

capable of ultra low emissions for NO_x and CO [4]. The modern applications of transient porous burners include combustion of low-calorific fuels, VOC emission control with the possibility of heat recovery, and fuel reforming in the ultra-rich superadiabatic flames as studied by Kennedy et al. [5] and Drayton et al. [6].

The presence of a high conductivity, high specific heat solid phase make it possible to employ porous combustion in surface combustor–heaters. The porous matrix is capable of retaining the heat produced by the reaction and transferring it to a cold body (heat exchanger). This significantly enhances the efficiency of the heat extraction from the combustion zone.

Historically the research on heat extraction from porous media burners was directed towards the steady state configuration. Typical examples are radiant burners [7,8] and surface combustor heaters, where coolant tubes are embedded in the porous matrix [9–11]. Nevertheless the transient approach offers advantages despite its higher degree of complexity.

The main problem arising from the unsteady nature of this phenomenon is that a method to confine the combustion in a practical burner has to be engineered. The reciprocal flow burner (RFB) configuration represents an extremely simple and effective way to achieve this result. In the RFB the direction of the flow is periodically reversed allowing the combustion zone to be restricted in a finite reactor though maintaining its transient behavior. The RFB systems have been recently an object of both numerical [12] and experimental investigations [13].

In the present work, a numerical model is employed to investigate the possibility of using RFB as a process heater. A new concept of heat extraction strategy is tested utilizing a heat exchanger made of two separate components embedded in the terminal sections of a porous matrix.

2. Numerical model

2.1. Statement of the problem

The geometrical and thermal characteristics have been selected to resemble an existing RFB whose schematic is shown in Fig. 1. The burner consists of a quartz tube of length $L = 0.5$ m and internal diameter $D = 76.4$ mm filled with spherical alumina pellets ($d = 5.6$ mm). The resulting packed bed has a porosity $\varepsilon = 0.4$. A thick insulation layer surrounds the tube making radial thermal gradients inside the burner negligible and giving the system efficient heat storage capability.

Two heat exchangers are embedded in the terminal sections of the reactor for a length $L_{ex} = 12$ cm. The device operates as follows. An external heat source progressively raises the temperature of the porous bed.

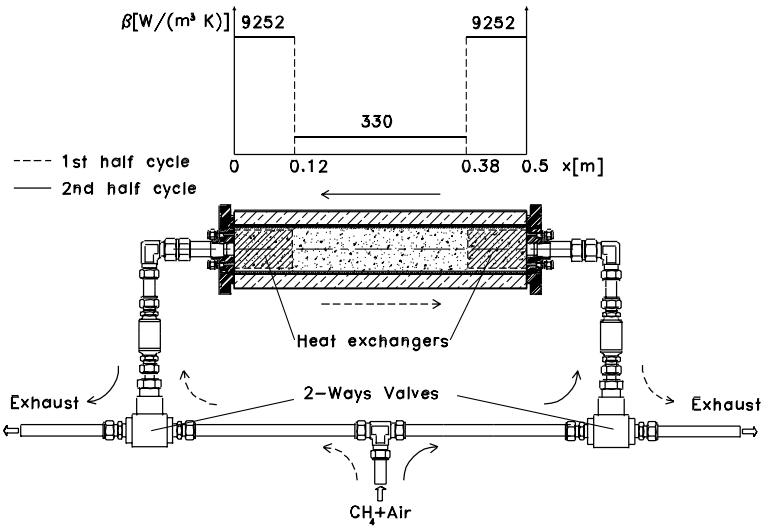

Fig. 1. Schematic of the RFB.

When the temperature sufficient to initiate the combustion is reached (≈900 °C), the external heat source is removed and a mixture of methane and air is allowed to flow into the burner. The direction of the flow is then switched periodically. The valve switching time is much less than a half cycle. Further, valve switching is assumed to be instantaneous in the current numerical study. The temperature profile modifies with time slowly approaching an asymptotic periodic behavior.

The selected RFB parameters represent an existing burner used in the experimental research on RFB combustion without heat extraction. The detailed description of the experimental setup is omitted here due to the space limitations. Further experimental research is planned to compare and validate numerical results presented here.

2.2. Governing equations

The temperature distribution as well as the species mass fractions inside the porous medium is considered to have a one-dimensional distribution. The solid and gas phase are allowed to have different temperatures. The gas phase is considered to be a mixture of only two generalized species: the reactants and the products:

$$\text{Reactants } [CH_4 + 2\varphi^{-1}(O_2 + 3.76N_2)] \Rightarrow \text{Products } [CO_2 + 2H_2O + 2(\varphi^{-1} - 1)O_2 + 2\varphi^{-1}3.76N_2]$$

This simplification reduces the number of variables necessary to describe the gas composition to one greatly reducing the computational time. The chemical reaction is descried by a single-step first order Arrhenius type reaction. The number of unknown 1-D functions is then restricted to three: $T_s(x)$, $T_g(x)$, and $y_p(x)$. Where $T_s(x)$ is the temperature of the porous matrix, $T_g(x)$ is the gas temperature, and y_p is the mass fraction of the products. The three time-dependent differential equations needed to find the solution are:

1. Solid phase energy conservation equation

$$(1-\varepsilon)c_s\rho_s\frac{\partial T_s}{\partial t} = \frac{\partial}{\partial x}\left(\left[k_s^* + k_r\right]\frac{\partial T_s}{\partial x}\right) + h_v(T_g - T_s) - \beta(T_s - T_0) \quad (1)$$

2. Gas phase energy conservation equation

$$\varepsilon c_g\rho_g\frac{\partial T_g}{\partial t} = \varepsilon\frac{\partial}{\partial x}\left(\left[k_g + (c_g\rho_g)D_{ax}\right]\frac{\partial T_g}{\partial x}\right) - \varepsilon c_g\rho_g v_g\frac{\partial T_g}{\partial x} + h_v(T_s - T_g) + \varepsilon H_{chem}W \quad (2)$$

3. Species conservation equation

$$\rho_g\frac{\partial y_p}{\partial t} = \frac{\partial}{\partial x}\left([D + D_{ax}]\frac{\partial y_p}{\partial x}\right) - \rho_g v_g\frac{\partial y_p}{\partial x} + W \quad (3)$$

where product mass production rate per unit volume W is given by the Arrhenius law:

$$W = \rho_g(1 - y_p)A_f\exp(-E_a/RT) \quad (4)$$

The activation energy and pre-exponential factor are $E_a/R = 24{,}358$ K, $A_f = 2.6$ E8 s^{-1} as suggested by Turns [14]. The heat of the reaction is computed as:

$$H_{chem} = \gamma\text{LHV} \quad (5)$$

The continuity equation was used in the form

$$\frac{\partial \rho v_i}{\partial x} = 0 \tag{6}$$

The radiative heat transfer is described by a radiant conductivity model [15]:

$$k_r = 4Fd\sigma T_s^3 \tag{7}$$

where the radiative heat exchange factor F is assumed to be 0.5. This value was estimated as the average value over the characteristic temperature interval for the considered packing composed of alumina pellets. The volumetric convective heat transfer coefficient h_v is used in the form suggested by Wakao and Kaguei [16]:

$$h_v = \left(\frac{6\varepsilon}{d^2}\right) k_g Nu \tag{8}$$

where Nusselt number is given by as:

$$Nu = 2 + 1.1 Pr^{1.3} Re^{0.6} \tag{9}$$

The heat flux through the burner walls is considered to be proportional to the temperature difference $(T_s - T_0)$ by the time-independent factor of β. The radial temperature gradient inside the packed is assumed to be negligible due to high dispersive and radiant conductivity of the porous media leading to essentially one dimensional problem formulation. The wall heat loss coefficient will be the subject of further discussion in the following sections.

Both energy conservation equations are similar to conventional homogeneous phase equations except for the interphase heat exchange term. It is worth noting also that both the heat and mass transfer phenomena are enhanced by the dispersion. The axial dispersion coefficient D_{ax} is given in the form $D_{ax} = 0.5 d v_i$ [16].

The gas conductivity is evaluated assuming a Lewis number equal to unity. The heat capacity, the thermal conductivity and the density of the porous matrix are assumed to be constant with respect to the temperature. To take into account the temperature dependence of the gas properties (c_g, k_g) the Chemkin [17] and Transport [18] subroutine libraries are used.

The analytical model described in the present section is basically similar to one used by Hannamura and Echigo [12] although some terms in several equations are refined; e.g., the dispersion effect is taken into account, the convective heat transfer coefficient is related to the local properties of the flow, and most of the thermodynamic and physical properties are considered temperature dependent. On the other hand the radiant flux calculation is simplified. The main introduced feature is the heat loss/heat extraction term.

2.3. Boundary conditions

The boundary conditions are imposed as follows:

$$\begin{aligned} &T_g(0) = T_0; \quad k_s^*(x<0) = k_r(x<0) = 0; \quad y_p(0) = 0 \\ &\frac{\partial T_g}{\partial x}(L) = 0; \quad k_s^*(x>L) = k_r(x>L) = 0; \quad \frac{\partial y_p}{\partial x}(L) = 0 \end{aligned} \tag{10}$$

Please note that all the boundary conditions are valid when the flow is moving from $x = 0$ to $x = L$. When the direction of the flow is reversed the boundary conditions at $x = 0$ and $x = L$ have to be swapped. An adiabatic boundary assumption is made meaning that no heat is transferred from the porous matrix boundary to the adjacent environment by conduction and radiation. This hypothesis is reasonable since the conduction and radiant heat fluxes at the reactor end are negligible if compared to the convective one.

2.4. Heat extraction

The presence of the heat exchangers embedded into the terminal sections of the reactor is simulated by imposing a non-uniform β distribution. Therefore a smaller value of the wall heat loss coefficient is used for the central zone, whereas a higher value is imposed in the areas cooled by the heat exchangers. The numerical value of β were evaluated experimentally to be: $\beta = 330$ W/m^3 K, in the heat extraction-free central section and $\beta_{ex} = 9200$ W/m^3 K in the heat extraction sections. The instantaneous extracted power is computed by integrating the heat flux through walls over the heat extracting sections.

$$P_{ex} = \int_0^{L_{ex}} \beta_{ex}(T_s(x) - T_0)\,dx + \int_{L-L_{ex}}^{L} \beta_{ex}(T_s(x) - T_0)\,dx \tag{11}$$

After averaging this instantaneous value over a number of cycles, the efficiency η can be computed as:

$$\eta = \frac{\overline{P}_{ex} A}{\gamma \dot{m} \mathrm{LHV}} \tag{12}$$

The global energy balance of the system can be represented as:

$$\overline{P}_{ex} = P_{chem} - \overline{P}_{walls} - \overline{P}_{conv} \tag{13}$$

For given realistic values of β_{ex} and L_{ex} the last term of Eq. (13) is negligible if compared to the other two meaning that almost all the energy loss is going through the reactor walls.

2.5. Solution method

The problem does not allow a steady state solution, due to periodic switching of the flow direction. A time

integration of the governing equations is to be performed. The Eqs. (1)–(3) are characterized by a strong numerical stiffness due to the coexistence of a very fast phenomenon, the chemical reaction, and a slow process of heat transfer in the porous media. To overcome this stiffness the solution of the equations at each time-step is split into two stages:

1. Solution of the steady state gas phase energy equation and species conservation equation for a constant solid temperature profile given by the previous integration step;
2. Time integration of the solid phase and gas phase energy equations for a constant heat release computed in the previous stage.

This means that the reaction rate is computed through the solution of steady state equations assuming that the solid temperature distribution is constant. Then the reaction heat release profile (assumed to be constant over the time step) is inserted into the gas phase energy equation that is integrated in time along with the solid phase energy equation.

In order to reach a numerical solution, the equations are discredited using a finite difference scheme. The derivatives for the convective term are computed using backward differences. Central differences are used for the transport terms. The time integration is performed using a partially implicit method. Several runs were performed to determine the proper time-step. Finally, the time interval $\Delta t = 10$ s was chosen. The steady state solution is found through a damped Newton algorithm. Due to the small size of the reaction zone relative to the computational domain, an adaptive re-gridding procedure is implemented to optimize the grid point distribution. The flow reversal is simulated by periodically mirroring the solid temperature distribution over the reactor midpoint. In other words, instead the flow reversal the reactor itself is reversed with gas always flowing from $x = 0$ to $x = L$.

2.6. Simulation

The discussed algorithm was implemented in a Fortran-90 code. The resulting program can simulate the operation of RFB for given flow parameters and an initial temperature distribution in the porous bed. The initial condition could be either a previous solution or a cold bed. In the last case a preheating phase is included to initiate the combustion. An additional uniform heating term is then introduced in the solid phase energy conservation equation, and removed as soon as the combustion starts.

The simulation is continued until a periodic behavior is reached. This condition, depending on initial conditions and on the velocity and heat content of the mixture, is reached after 5000–10,000 s of simulated time. The output of the program is the evolution in time of the temperature distribution in both solid and gas phase and in the product mass fraction profile. The output is post processed to determine the instantaneous and average power extracted from the reactor.

3. Results

Several series of simulations were run with the purpose of investigating the influence of the most essential parameters: equivalence ratio φ, filtration velocity v_f, wall heat losses coefficient β, and length of the heat exchangers L_{ex}. The role of the switching period was also analyzed but the results of this analysis will be omitted as the negligible effect of the switching time on the average reactor performance was obtained.

3.1. Evolution during the half cycle

The shape of the solid temperature distribution ($\varphi = 0.3$, $v_f = 20$ cm/s) at the beginning and the end of the half cycle is shown in Fig. 2. During the selected half cycle the gas is flowing from left to right. The power per unit volume transferred from the gas to the solid phase is included on the same graph to clarify the heat recuperation effect of the porous matrix. In the positive gradient section some heat is absorbed by the gas allowing it to reach the ignition temperature. Then in the reaction zone the gas delivers heat to the solid. In the central section the interphase heat transfer is close to zero because the thermal gradients are low and no reaction is occurring. Finally, in the negative gradient section, the heat is transferred from the gas phase to the solid.

The periodic configuration of the temperature profile in the RFB is basically M-shaped. The two low-temperature, low-gradients zones at the end of the burner are obviously due to the presence of the heat exchangers. The two temperature peaks correspond to the zones where the combustion takes place. Depending on the flow direction, ignition occurs in the proximity of the peak closest to the gas inlet. The central plateau is actually valley-shaped. Its depression is due to the wall heat losses.

At the beginning of the cycle, the right peak is higher than the left one because that was the flame location during the previous cycle. As the half cycle goes on, the temperature of the left peak increases supported by the combustion heat release while the right peak is diminishing due to the heat losses. The temperature profile after a half period is perfectly symmetric to the initial temperature profile. In Fig. 2, the gas temperature distribution is also plotted. It is noticeable that the thermal non-equilibrium between the two phases is fairly low.

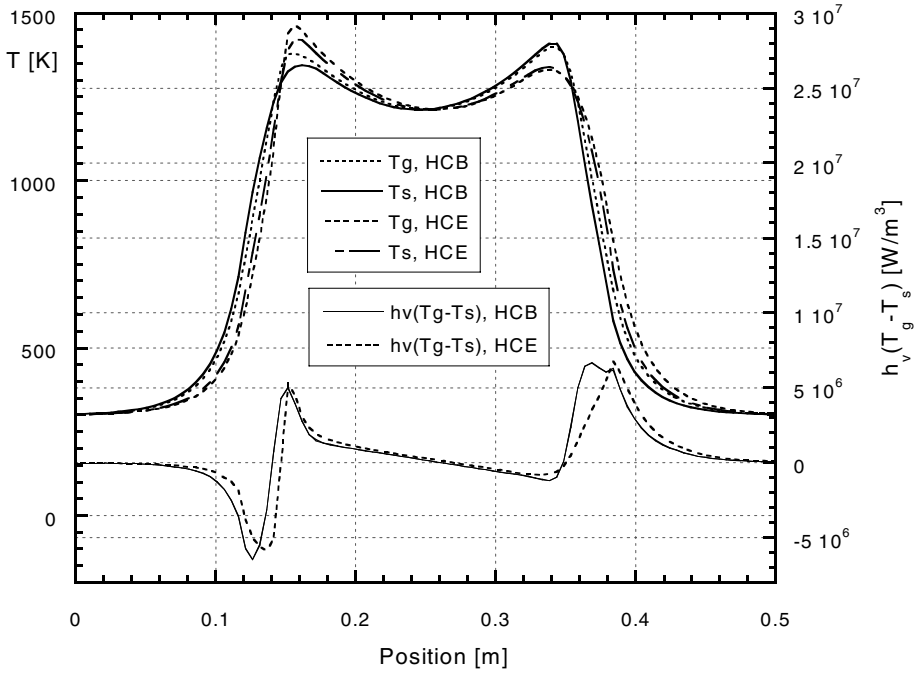

Fig. 2. Temperature evolution during half cycle of the RFB: $\varphi = 0.3$, $v_f = 20$ cm/s. The acronyms HCB and HCE stand for the half cycle beginning and the half cycle end.

Due to this reason only solid temperature profiles at the end of the cycle (gas flowing from left to right) are presented further.

The temperature evolution during the half cycle has a strong effect on the power extracted by the heat exchangers. When the gas is flowing from left to right, the convective action of the mixture actually cools the left heat exchanger while heating the right one. The situation is opposite with flow reversal. This result in strong fluctuations of the instantaneous power extracted from each heat exchanger. These fluctuations are shown in Fig. 3, along with the total power and the lost power. The sum of the powers extracted from the two heat exchangers is periodic but with a fairly small amplitude.

The temperature profiles (Fig. 2) and the extracted power variations (Fig. 3) are a result of evolution of the reactor temperature profile. This evolution is shown in Fig. 4 as a 3-D graph. The first 950 s correspond to the preheating stage. As soon as the combustion is initiated, two reaction zones start moving apart reaching the stable position at lateral zones cooled by the heat exchangers.

3.2. Influence of equivalence ratio

To determine the influence of the equivalence ratio a series of simulations were performed varying φ in the range from 0.15 to 0.7 with increment $\Delta\varphi = 0.5$. The filtration velocity was kept constant at 20 cm/s. In Fig. 5, the solid phase temperature distributions are plotted for several representative values of φ along with the volumetric heat release rate. The heat release rate is provided for qualitative and quantitative information about the position, intensity, and thickness of the reaction zone.

The equivalence ratio mainly affects the shape of the profile changing the lateral temperature gradients and the width of the central plateau. The lower the equivalence ratio the closer are the temperature peaks and the lower are the lateral temperature gradients. The maximum temperature in the reactor also increases with equivalence ratio, but this increase is fairly low. This effect further diminishes for low wall heat loss coefficients.

The average temperature in the central section of the reactor and the power lost through the walls are growing with the φ increase as the oblique sides of the trapezoidal temperature profile become steeper. This effect is not linearly proportional to the heat content of the mixture, as shown in Fig. 6. As a consequence for the lowest equivalence ratio studied, the lost power is even higher then the extracted power ($\eta < 50\%$), but then P_{ex} grows steeply while P_{lost} increases at a much slower rate. As a result the efficiency grows sensibly from less than 50% at $\varphi = 0.15$ to more than 75% at $\varphi = 0.7$.

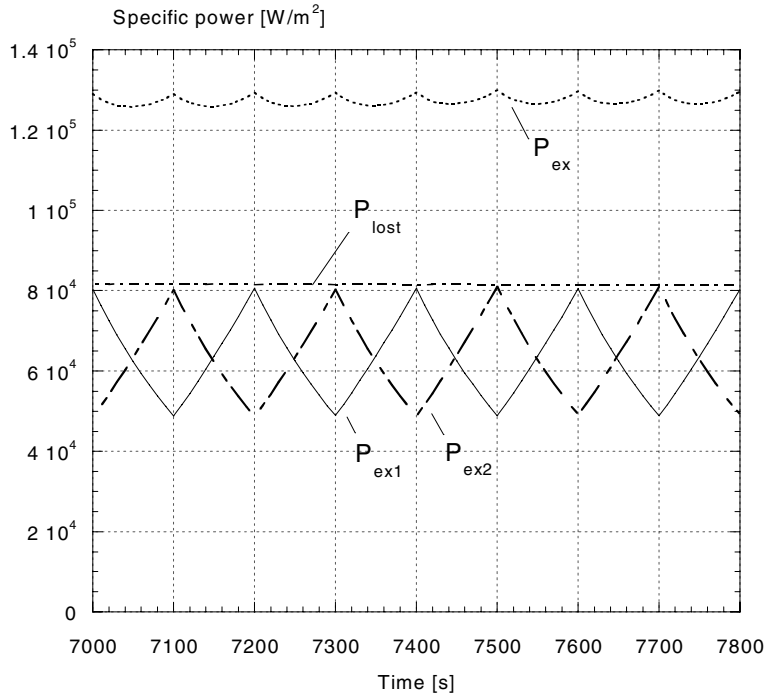

Fig. 3. Total extracted power, lost power and power extracted from the left (1) and the right (2) heat exchanger as a function of time.

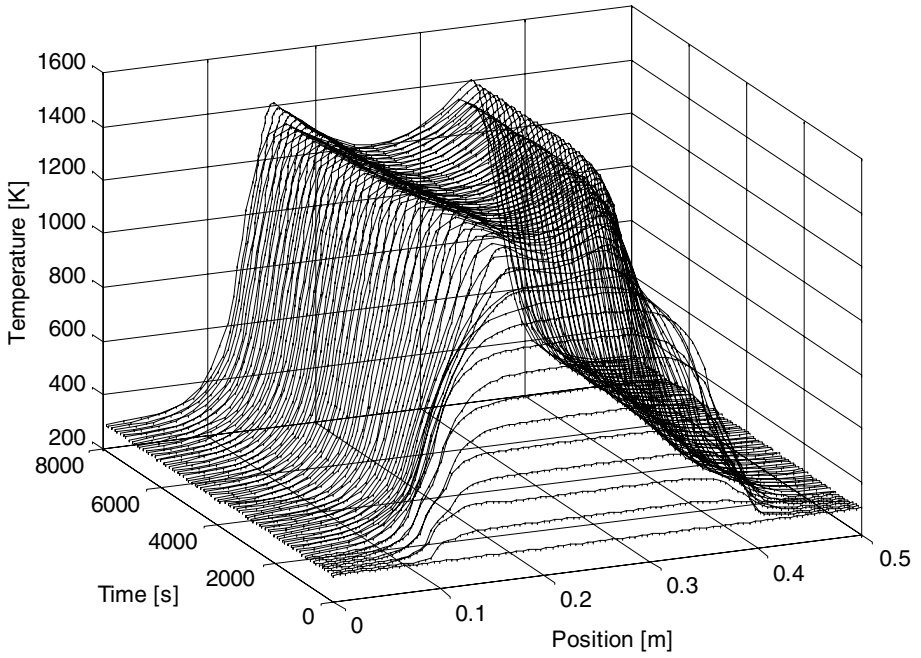

Fig. 4. Evolution of the temperature reactor inside the RFB. The external heat source is used for initial 950 s and then removed after ignition of the mixture.

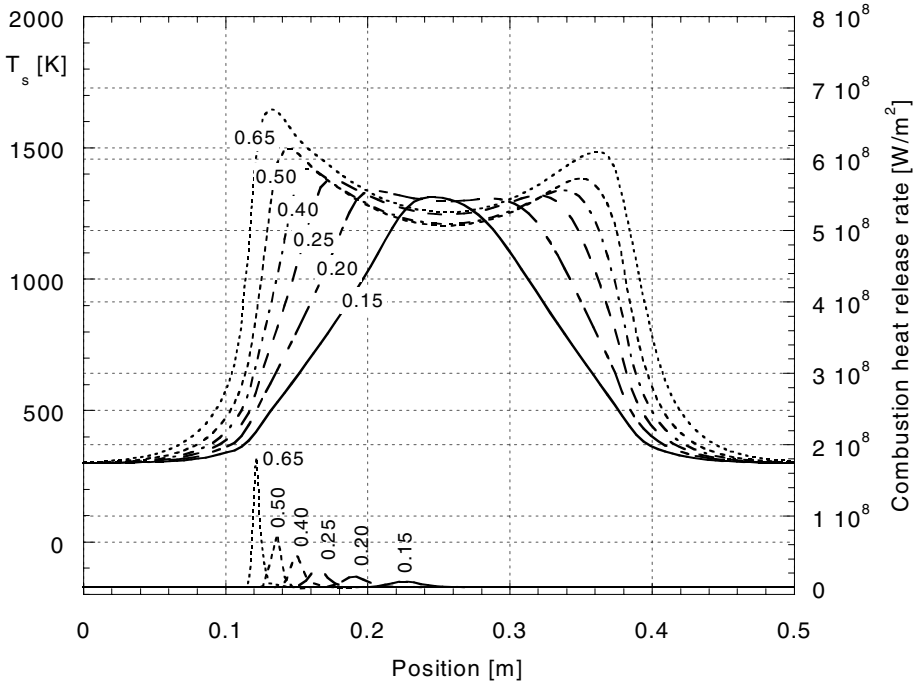

Fig. 5. Effect of equivalence ratio on temperature profile at the RFB. Numbers show equivalence ratio; filtration velocity is 20 cm/s.

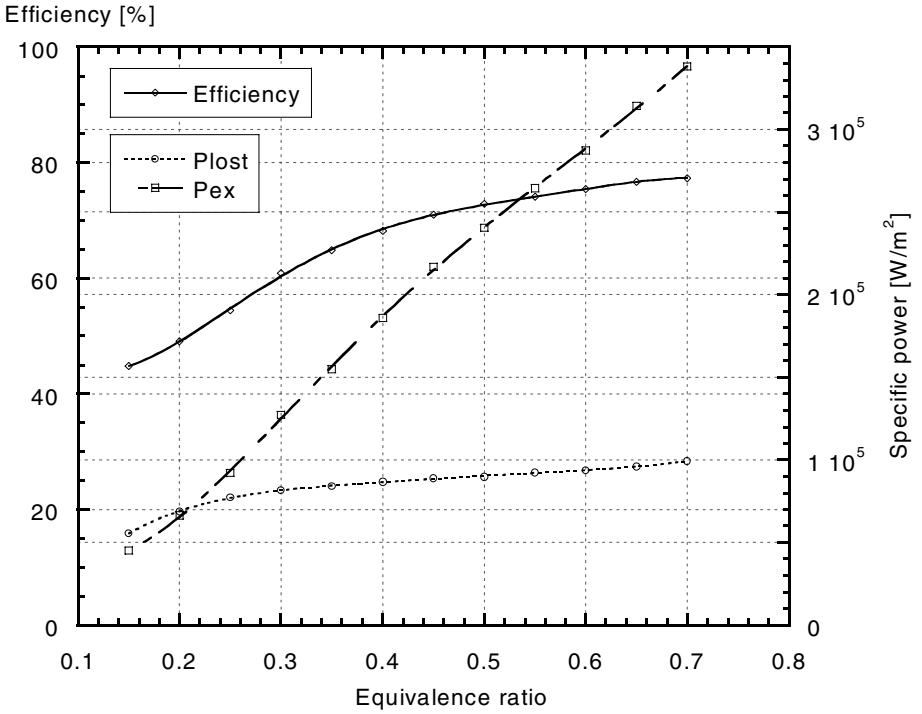

Fig. 6. Variation of efficiency, extracted and lost power with equivalence ratio ($v_f = 20$ cm/s).

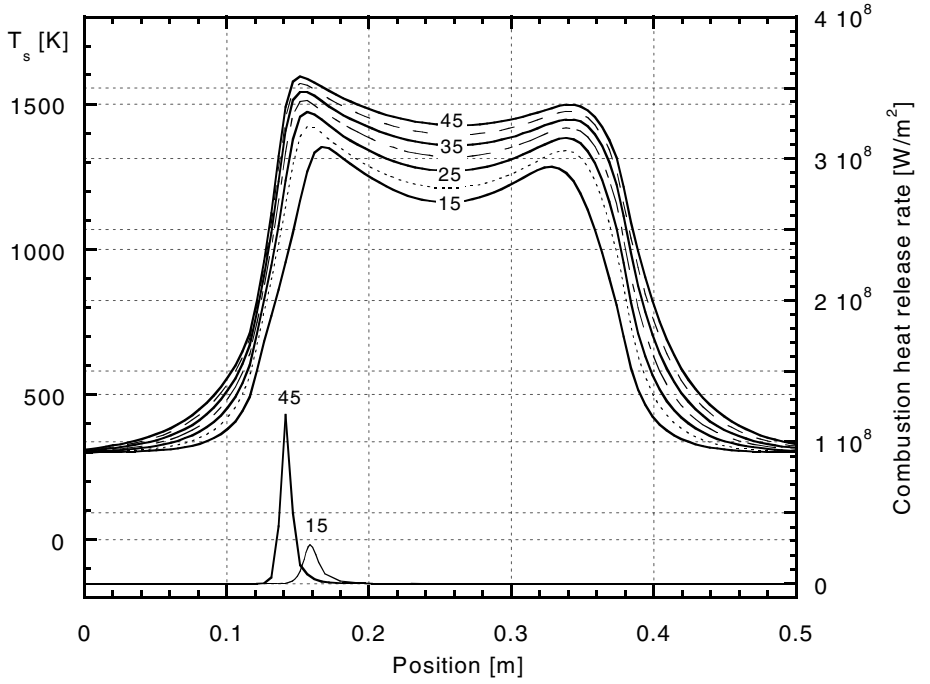

Fig. 7. Effect of filtration velocity on temperature profile in the RFB. Numbers show filtration velocities in cm/s. Equivalence ration is equal to 0.3.

3.3. Influence of the filtration velocity

A series of simulation was performed varying the filtration velocity from 15 to 45 cm/s with increments $\Delta v_f = 5$ cm/s. The equivalence ratio was kept constant at $\varphi = 0.3$. The obtained temperature profiles are shown in Fig. 7. In contrast to variation of equivalence ratio, varying the filtration velocity seems to have very little effect on the shape of the temperature distribution. In fact, both the locations of the combustion zones and the lateral thermal gradients remain fairly unchanged.

The influence of the filtration velocity appears to be limited to increase of the central plateau temperature. It is noticeable also that the average temperature in the heat extraction zones increases with v_f due to increase of the power load.

The average temperature in the central section is higher for higher filtration velocities. This is due to the growth of the height of the trapezoidal temperature distribution. Concurrently, the lost power increases, but again, not proportionally to the power load (Fig. 8). Similarly to the case of φ variation, the efficiency grows from $\eta = 51\%$ at $v_f = 15$ cm/s to $\eta = 78\%$ at $v_f = 45$ cm/s.

3.4. Influence of the wall heat loss coefficient

The wall heat loss coefficient β expresses the proportionality coefficient between the integral of the temperature in the central section of the reactor and the lost power. A series of simulations was performed varying β in the range from 130 to 430 W/m^3 K. As shown in Fig. 9, the lateral thermal gradients seem to be unaffected by β. On the other hand the zone between the peaks significantly changes its morphology. For low β the central plateau resemble a real plateau and is almost flat. Increase of β leads to the sensible decrease of the midpoint temperature. The peak temperature values are also slightly lowered by β increase. As expected the efficiency decreases with β in a fairly linear fashion, dropping from $\eta = 77\%$ at $\beta = 130$ W/m^3 K to $\eta = 54\%$ at $\beta = 430$ W/m^3 K (Fig. 10).

3.5. Influence of the reactor length

For fixed equivalence ratio ($\varphi = 0.3$) and filtration velocity the reactor length was varied in the range from 6 to 8 cm. This corresponds to decrease of the insulated reactor portion from 76% to 28% of its full length. As shown in Fig. 11, the change of the heat exchangers length shifts the two high thermal gradient zones without modifying their slope. The longer the heat exchanger the closer to each other the two temperature peaks are. For $L_{ex} = 18$ cm these zone almost converge to the single peak. As the central plateau narrows down, the temperature in the reactor midpoint increases; the height of the temperature peaks increases.

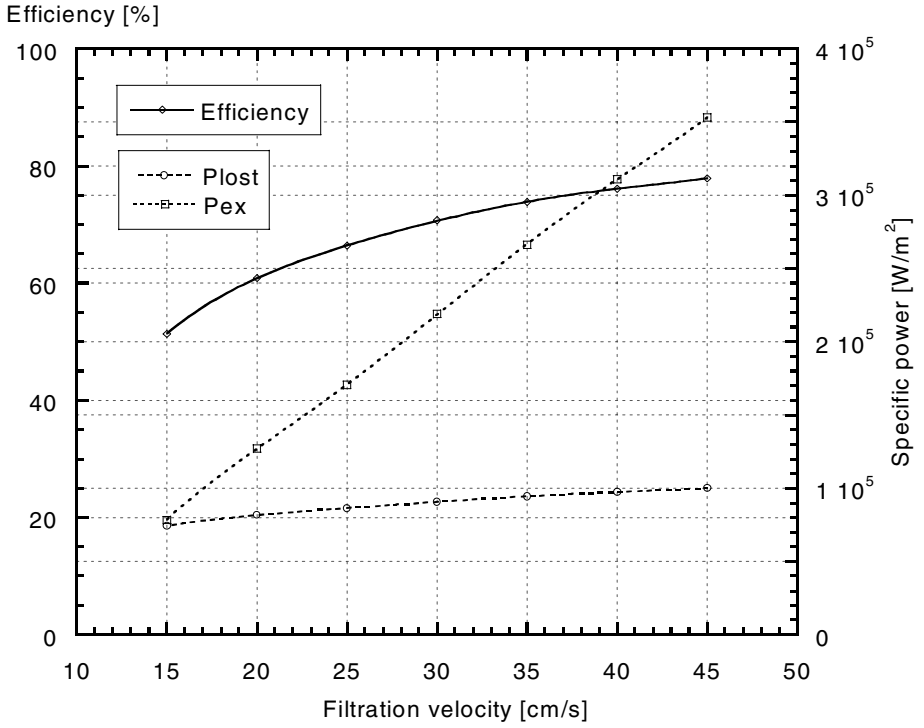

Fig. 8. Variation of efficiency, extracted and lost power with filtration velocity ($\varphi = 0.3$).

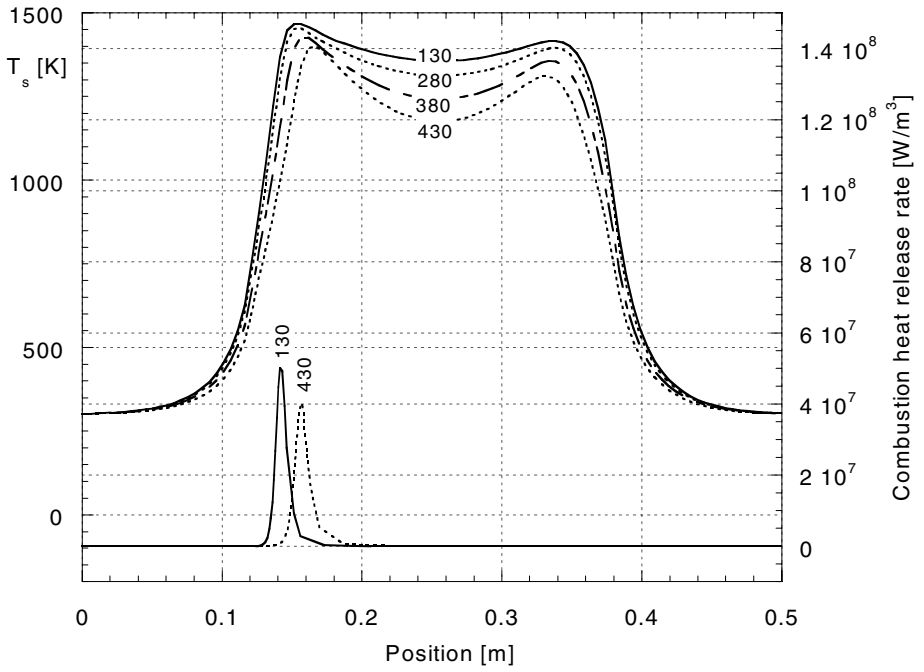

Fig. 9. Effect of the wall heat losses coefficient of the RFB temperature profile. Numbers show β in W/m^3 K. Filtration velocity—20 cm/s, equivalence ratio—0.3.

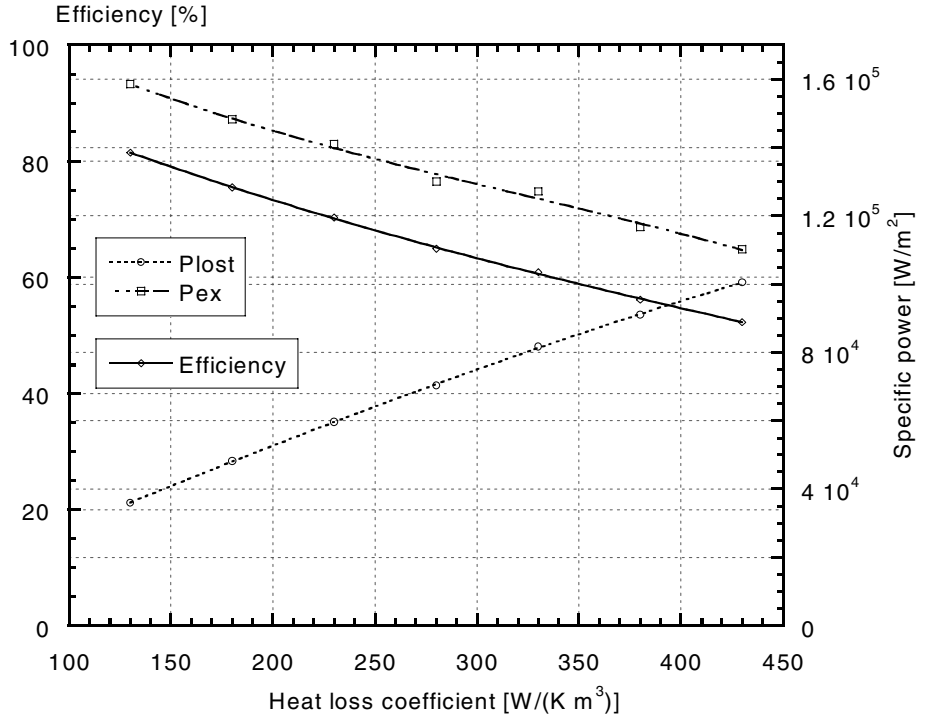

Fig. 10. Variation of efficiency, extracted and lost power with β ($v_f = 20$ cm/s, $\varphi = 0.3$).

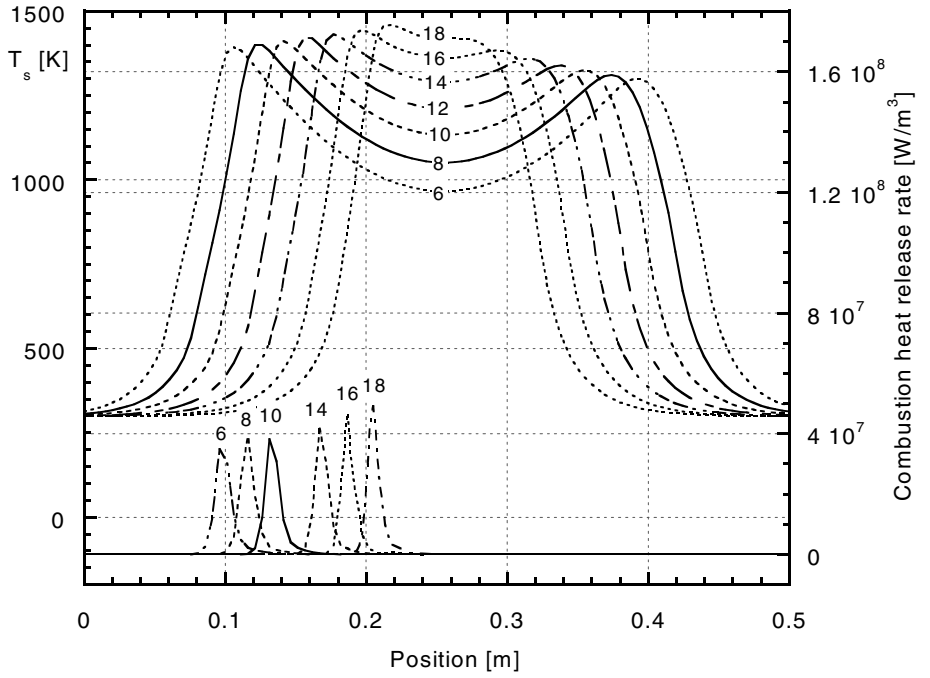

Fig. 11. Effect of the heat exchanger length on the RFB temperature profile. Numbers show L_{ex} in cm. Filtration velocity—20 cm/s, equivalence ratio—0.3.

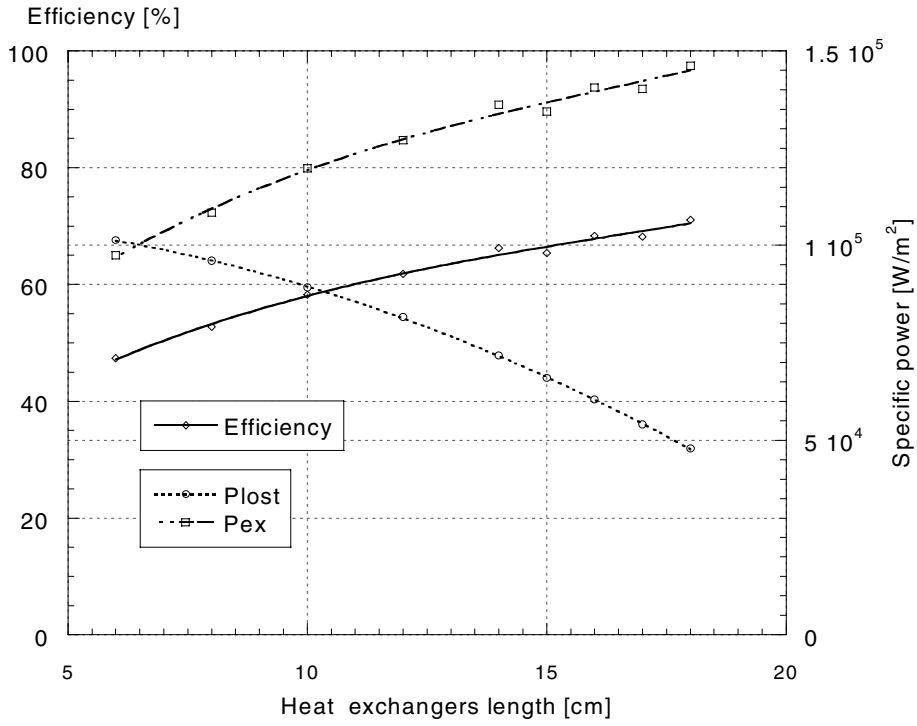

Fig. 12. Variation of efficiency extracted and lost power with L_{ex} ($v_f = 20$ cm/s, $\varphi = 0.3$).

The efficiency, lost and extracted power are plotted in Fig. 12. Decreasing the non-insulated sections of the reactor has the obvious effect of reducing the amount of heat lost through walls, increasing the efficiency from $\eta = 49\%$ at $L_{ex} = 6$ cm to $\eta = 75\%$ at $L_{ex} = 18$ cm.

Although this seems to be the most effective way to increase the reactor efficiency, some limitations apply. In fact, L_{ex} has an upper limit due to the fact that the distance between the two peaks has to be greater than (or equal to) zero, or the reaction will extinguish. This upper limit differs for various lateral thermal gradients and for various equivalence ratios. Once the length of the heat exchangers is fixed the minimum operative equivalence ratio is also fixed and vise versa.

4. Conclusions

A numerical model was developed for predicting the thermal structure of combustion in a RFB with two heat exchangers embedded in its lateral sections. The relevant equations are integrated in time until the periodic behavior is reached defining the temperature distribution in both solid and gas phase, the chemical reaction zone location and thickness. The extracted and lost power is computed to evaluate the system efficiency. A sensitivity study is performed to determine how the behavior of the system is affected by variation of equivalence ratio, filtration velocity, wall heat loss coefficient and length of the heat exchanger. The simulation show that the RFB is able to burn mixtures with equivalence ratios as low as $\varphi = 0.15$ ($v_f = 20$ cm/s). On the other hand the presence of heat exchangers confines the reaction zones in the central insulated section, allowing stable combustion with virtually any equivalence ratio. The temperature profile has typical trapezoidal shape with a minimum at the reactor midpoint. The lateral gradients flatten out with decrease of equivalence ratio until trapezium degenerates into a triangle. The triangular temperature distribution represents the extinction limit. The filtration velocity increases the plateau temperatures. Both increasing β and decreasing L_{ex} lowers the midpoint temperature minimum.

Using simulation parameters resembling an existing RFB the efficiency is predicted to be between 50% and 80%. Higher efficiencies correspond to higher equivalence ratios, higher filtration velocities, lower β and higher heat exchanger lengths.

Acknowledgements

The authors wish to acknowledge the support of this work by the National Science Foundation grant CTC 9812905. One of the authors (FC) was partially supported by an Air Liquide Fellowship.

References

[1] V.S. Babkin, Filtration combustion of gases, present state of affairs and prospects, Pure Appl. Chem. 65 (1993) 335–344.

[2] Y.M. Laevskii, V.S. Babkin, Filtration combustion of gases, in: Y. Matros (Ed.), Propagation of Heat Waves in Heterogeneous Media, Nauka, Novosibirsk, 1982, pp. 108–145.

[3] S.A. Zhdanok, L.A. Kennedy, G. Koester, Superadiabatic combustion of methane air mixtures under filtration in packed bed, Combust. Flame 100 (1995) 221–231.

[4] J.P. Bingue, A.V. Saveliev, A.A. Fridman, L.A. Kennedy, NO_x and CO emissions of lean and ultra-lean filtration combustion of methane/air mixtures in inert porous media, in: Proceedings of the Fifth International Conference on Technologies and Combustion for a Clean Environment, Lisbon, Portugal, 1998, pp. 1361–1367.

[5] L.A. Kennedy, A.A. Fridman, A.V. Saveliev, Superadiabatic combustion in porous media: wave propagation, instabilities, new type of chemical reactor, Fluid Mech. Res. 22 (1995) 1–26.

[6] M.K. Drayton, A.V. Saveliev, L.A. Kennedy, A.A. Fridman, Syngas production using superadiabatic combustion of ultra-rich methane–air mixtures, Proc. Combust. Inst. 27 (1998) 1361–1367.

[7] A.A. Mohamad, R. Viskanta, S. Ramadhyani, Numerical predictions of combustion and heat transfer in a packed bed with embedded coolant tubes, Combust. Sci. Technol. 96 (1994) 387–407.

[8] M.D. Rumminger, R.W. Dibbie, N.H. Heberle, D.R. Crosley, Gas temperature above a radiant porous burner: comparison of measurements and model predictions, Proc. Combust. Inst. 26 (1996) 1755–1762.

[9] T.W. Tong, S.B. Sathe, Heat transfer characteristics of porous radiant burners, J. Heat Transfer 113 (1991) 387–407.

[10] T.Y. Xiong, M.J. Khinkis, F.F. Fish, Experimental study of a high-efficiency, low emission porous matrix combustor-heater, Fuel 74 (11) (1995) 1641–1647.

[11] Y. Xuan, R. Viskanta, Numerical investigation of a porous matrix combustor–heater, Numer. Heat Transfer, Part A 36 (1999) 359–374.

[12] K. Hannamura, R. Echigo, S. Zhdanok, Superadiabatic combustion in porous media, Int. J. Heat Mass Transfer 36 (13) (1993) 3201–3209.

[13] L.A. Kennedy, A.V. Saveliev, A.A. Fridman, Transient filtration combustion, in: Proceedings of Mediterranean Combustion Symposium, Antalya, Turkey, 1995, pp. 105–128.

[14] S.R. Turns, An Introduction to Combustion, McGraw-Hill, Boston, 1996, p. 137.

[15] M. Kaviany, Principles of Heat Transfer in Porous media, Springer-Verlag, New York, 1995, pp. 340–345.

[16] N. Wakao, S. Kaguei, Heat and Mass Transfer in Packed Beds, Gordon and Breach Science Publications, New York, 1982, pp. 86–150.

[17] R.J. Kee, F.M. Rupley, J.A. Miller, CHEMKIN-II a Fortran chemical kinetics package for the analysis of gas-phase chemical kinetics, Sandia National Laboratories, Report #SAND89-8009, 1989, pp. 1–126.

[18] R.J. Kee, G. Dixon-Lewis, J. Warnatz, M.E. Coltrin, J.A. Miller, A Fortran computer package for the evaluation of gas-phase, multicomponent transport properties, Sandia National Laboratories, Report #SAND86-8246, 1986, pp. 1–46.